SUPPORTING INFORMATION

Sequential delivery of doxorubicin and zoledronic acid to breast cancer cells by CB[7]-modified iron oxide nanoparticles

Farah Benyettou,[†] *Marwa Alhashimi,* [†] *Matthew O'Connor* [†] *Renu Pasricha,* [†] *Jeremy Brandel,*[‡] *Hassan Traboulsi,*[Δ] *Javed Mazher,*[ʌ] *John-Carl Olsen*[◊] *Ali Trabolsi*[†]*

†New York University Abu Dhabi, PO Box 129188, Abu Dhabi, United Arab Emirates, ‡ Equipe Reconnaissance et Procédés de Séparation Moléculaire, Université de Strasbourg, 67037, Strasbourg, France, Δ Chemistry Department, College of Sciences, King Faisal University – Al Ahsa, 31982, Kingdom of Saudi Arabia, ʌ Physics Department, College of Sciences, King Faisal University-Al Ahsa, 31982, Kingdom of Saudi Arabia ◊ Department of Chemistry, University of Rochester RC PO Box 270216, Rochester, NY 14607-0216, United States of America.

* ali.trabolsi@nyu.edu.

Iron concentration was deduced from UV-Visible absorption spectra recorded with an Agilent Technologies Cary 5000 Series UV-Vis-NIR Spectrophotometer in water at room temperature (298 K). Solutions were examined in 1 cm spectrofluorimetric quartz cells. The experimental error of the wavelength values was estimated to be ~1 nm. Infrared spectra were recorded on an Agilent Technologies Cary 600 Series FTIR Spectrometer using the ATR mode. Thermogravimetric analyses were performed on a TA SDT Q600 device. Emission spectra in water at room temperature were recorded on a Perkin Elmer LS55 Fluorescence Spectrometer using an excitation wavelength of 488 nm, which corresponds to the wavelength that absorbs maximally. Phase contrast and fluorescence images were observed on an Olympus FV1000MPE confocal scanning microscope. The nanoparticles were heated using a magneTherm (NanoTherics) system, a device that allows magnetic fluid and nanoparticle hyperthermia testing. Dynamic light scattering (DLS) measurements were performed on a Malvern Zetasizer NanoSeries to obtain the size and ζ-potential of the nanoparticles. Flow cytometry analyses were performed on Accuri C6 Flow Cytometer. All LC-MS/MS analyses were performed on an Agilent 6538

Agilent Quadrupole-TimeOfFlight spectrometer using the dual ESI source. Mass spectra were acquired and processed with Masshunter software. Mass spectrometry conditions were performed using direct infusion with a syringe pump. XPS was performed in single channel detection mode by using the Omicron ESCA-II system and Mg-Kα radiation.

1. NP Characterization

1.1. High resolution transmission electron microscopy (HRTEM).

High resolution transmission electron microscopy (HRTEM) images were obtained using a Talos F200X Scanning/Transmission Electron Microscope (STEM) equipped with CETA 16M camera and having a lattice-fringe resolution of 0.14 nm at an accelerating voltage of 200 kV. The high-resolution images of periodic structures were analyzed using TIA software. The samples for the HRTEM study were prepared on holey carbon film mounted on a copper grid. A drop of **NP** solution ([Fe]= 1.0×10^{-5} M) was spotted on the grid and allowed to dry overnight.

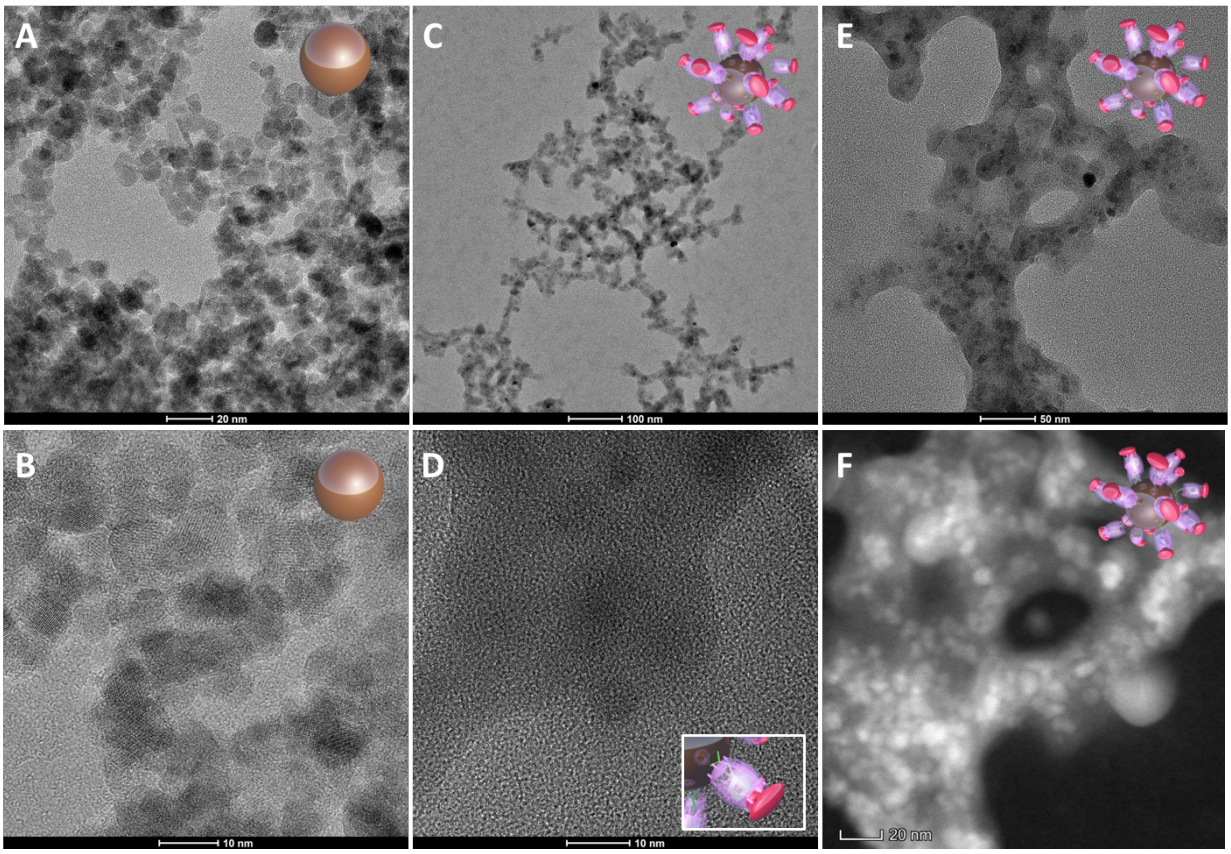

Figure S1. TEM and HRTEM images of **NPs** (A−B) and **DCZ-NPs** (C−E) and STEM image of **DCZ-NPs** (F).

1.2. Fourier transform infrared (FTIR) spectroscopy

The surface modification of **NPs** with Zol, CB[7] and Dox was confirmed and characterized by ATR-IR spectroscopy using an Agilent Technologies Cary 600 Series FTIR Spectrometer. The spectral data within the range of 4000 to 600 cm^{-1} were recorded, and 512 scans were averaged for each spectrum with a spectral resolution of 2 cm^{-1}. The spectrum of the background was recorded first and it was subtracted from the spectra of samples automatically.

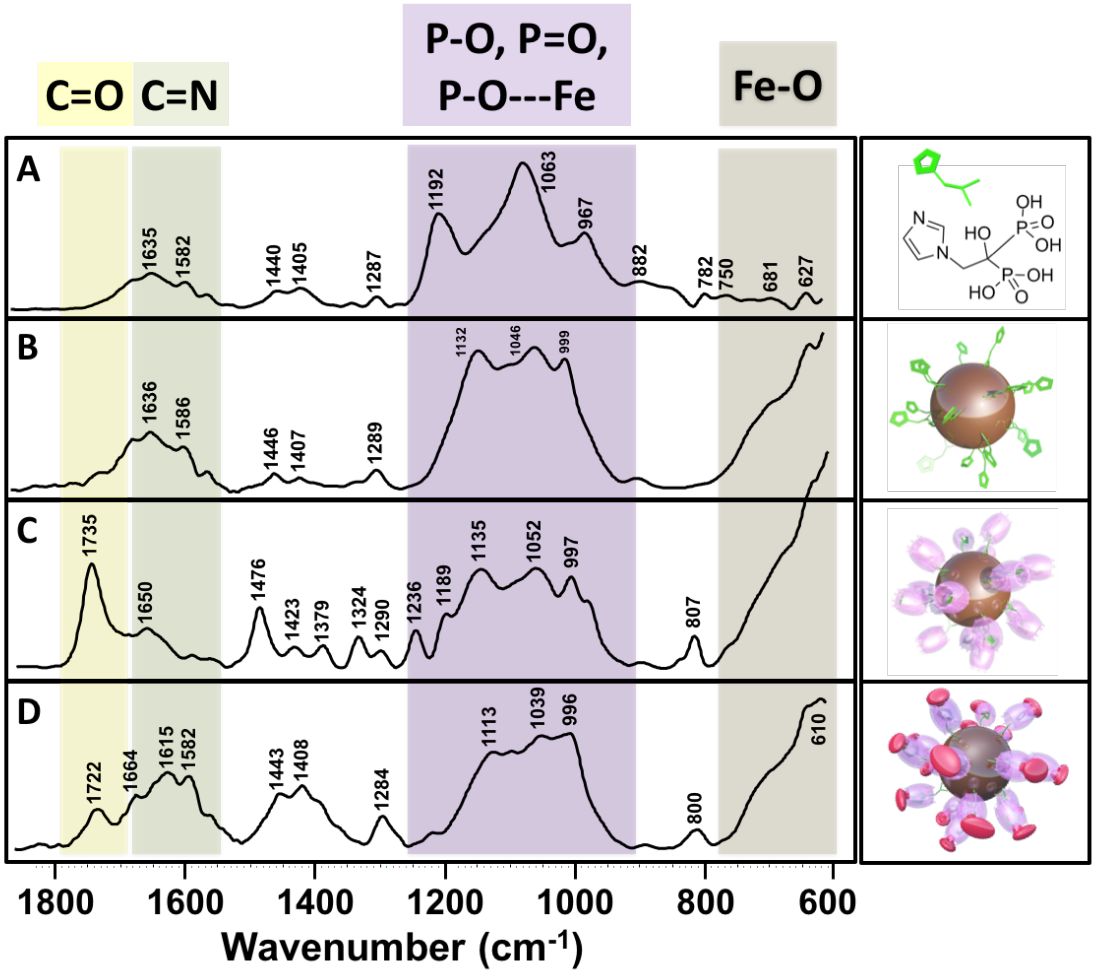

Figure S2. Comparison of the FTIR spectra of (A) free Zol, (B) **Z-NPs**, (C) **CZ-NPs** and (D) **DCZ-NPs**.

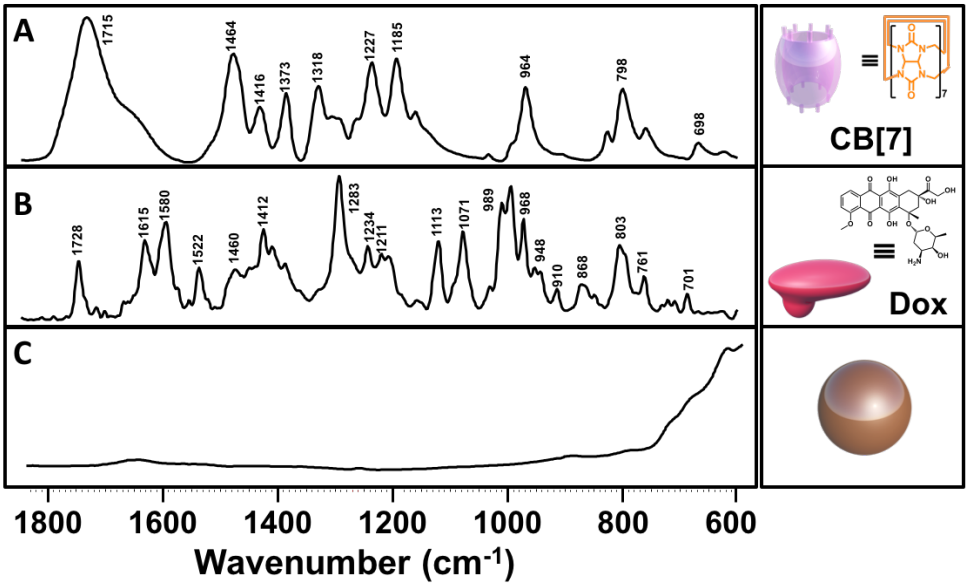

Figure S3. FTIR spectra of (A) free CB[7], (B) free Dox, and (C) uncoated **NPs**.

1.3. X-Ray Photoelectron Spectroscopy (XPS) analysis

XPS analysis was performed in order to investigate the elemental composition of the γ-Fe_2O_3 nanoparticles before and after functionalization. Prior to data recording, the samples were dried using ultra high vacuum, and the spectrometer calibration was thoroughly checked using the Ag 1s peak position. High resolution XPS data were obtained with an energy resolution of 0.05 eV and a dwell time of 0.2 s at an X-ray power of 50 W. All XPS spectra were analyzed using the CasaXPS software where deconvolution of the spectra into different components was carried out. Each spectrum was fitted by means of an iterative least-squares procedure with Gaussian bands.

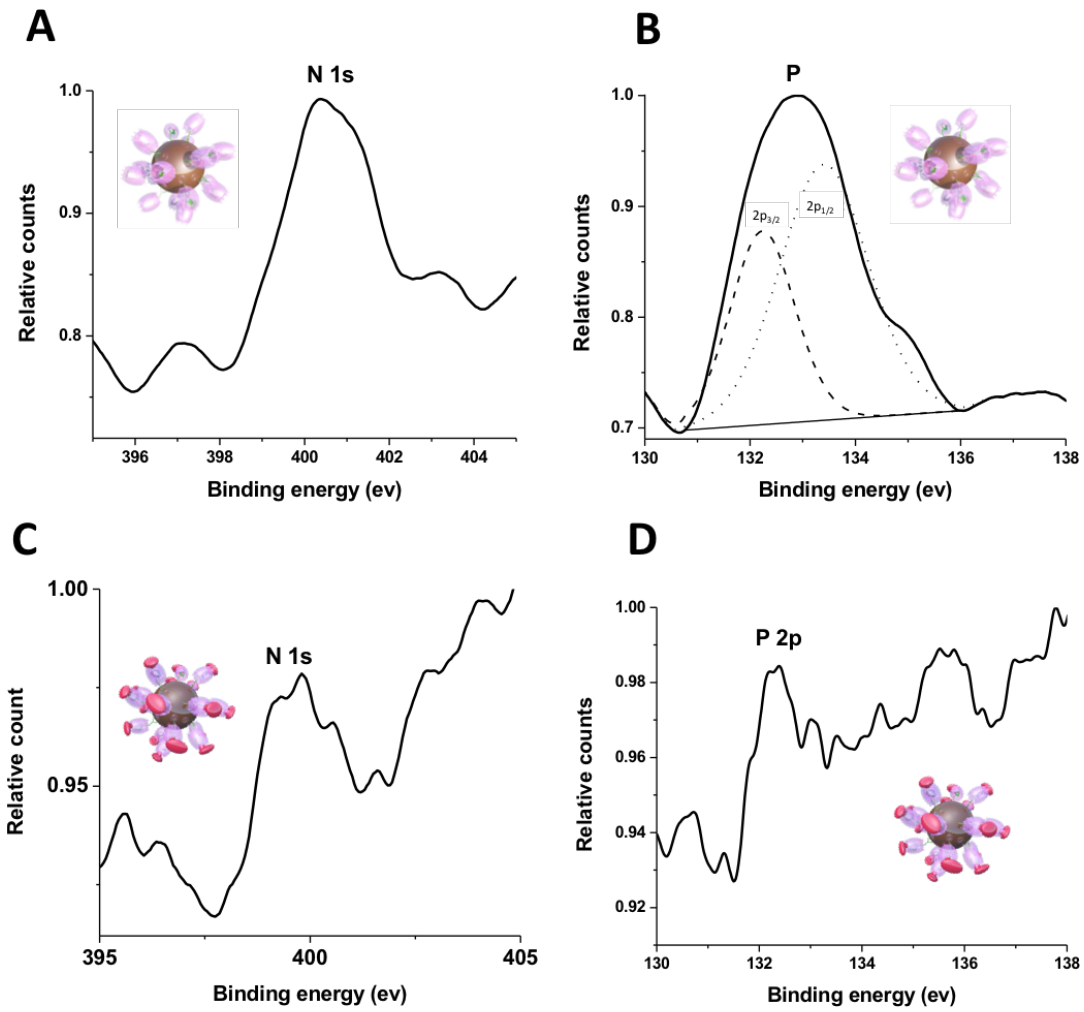

Figure S4. High resolution XPS spectra of nitrogen N 1s and phosphorus P 2p in **CZ-NPs** (A and B, respectively) and **DCZ-NPs** (C and D, respectively).

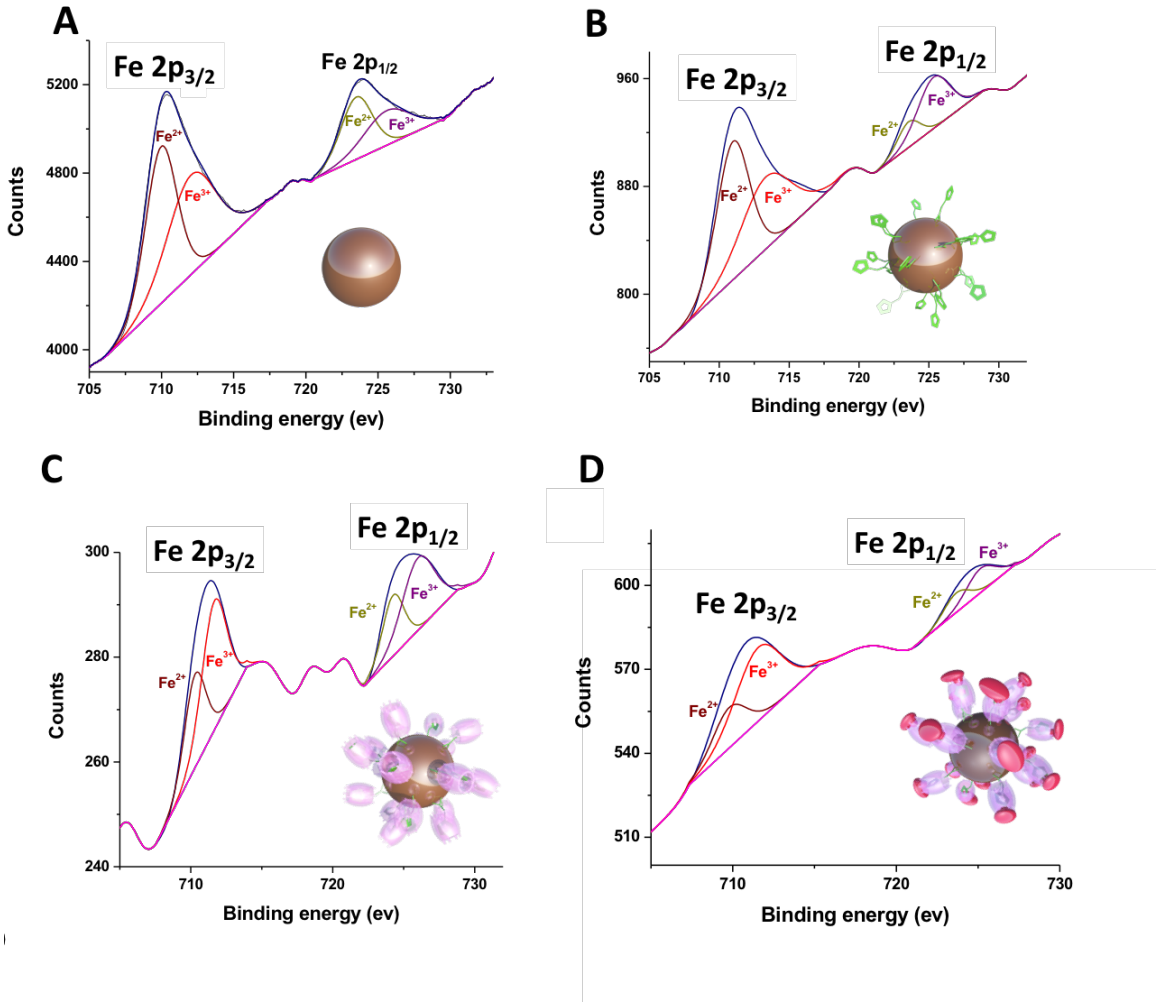

Figure S5. High resolution XPS spectra of Fe 2p in **NP** (A), **Z-NP** (B), **CZ-NP** (C) and **DCZ-NPs** (D).

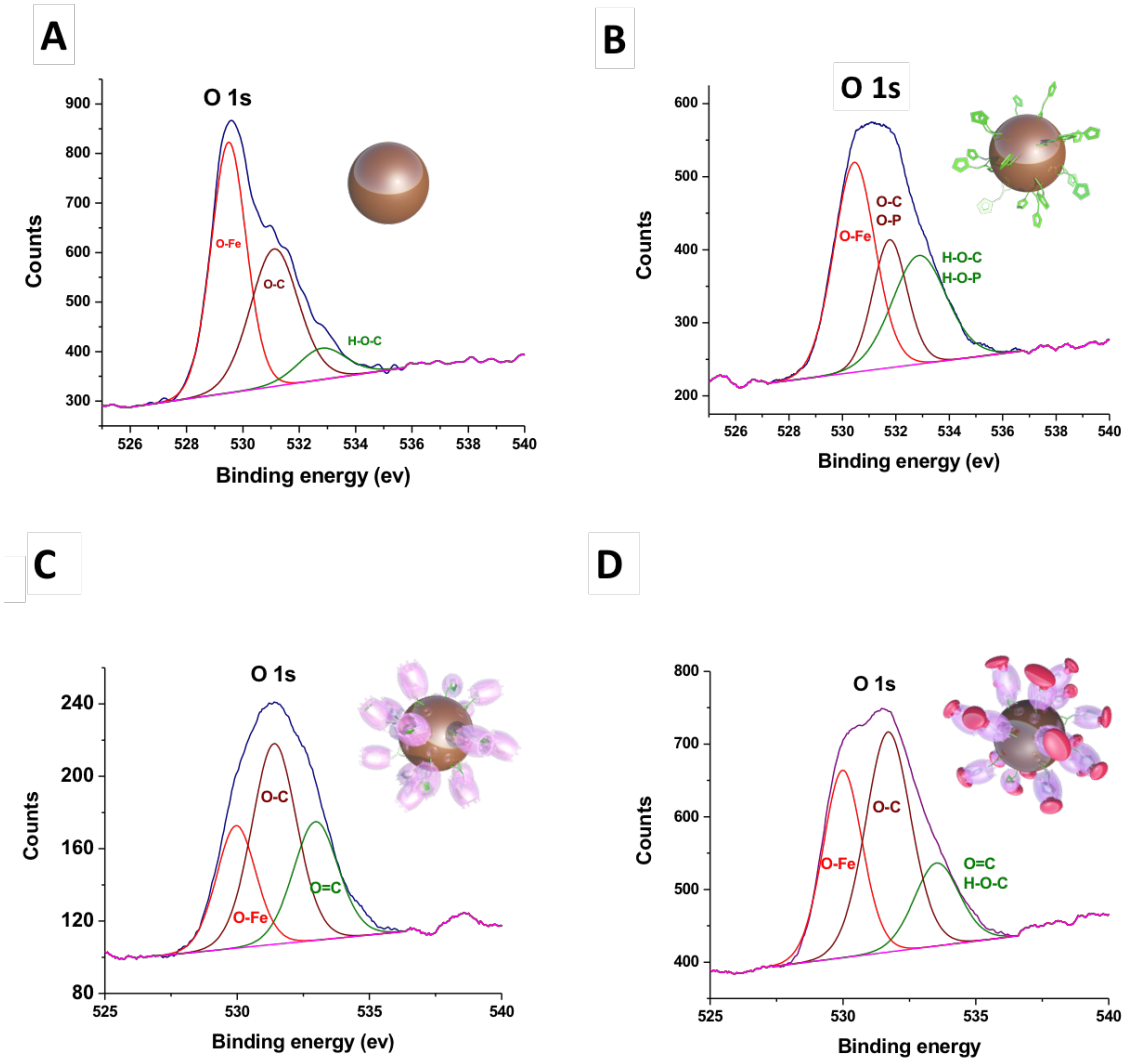

Figure S6. High resolution XPS spectra for O 1s in **NP** (A), **Z-NPs** (B), **CZ-NPs** (C) and **DCZ-NPs** (D).

1.4. Thermogravimetric analysis (TGA)

The weight percentage of each specie on the surface of **NPs** was determined by TGA. Solid samples (10 mg) under N_2(g) flux were characterized with a SDT Q600 TA Instruments analyzer at a heating rate of 5 ºC/min over a temperature range of 35–700 ºC. Figure S7 shows the weight losses of **NPs**, **Z-NPs**, **CZ-NPs** and **DCZ-NPs**. The initial sharp decrease in weight (30 ºC to 180 ºC) corresponds to the removal of physisorbed

water molecules. The second major loss (200 ºC to 600 ºC) corresponds to the removal of the organic layer (Zol; Zol and CB[7]; or Zol, CB[7] and Dox).

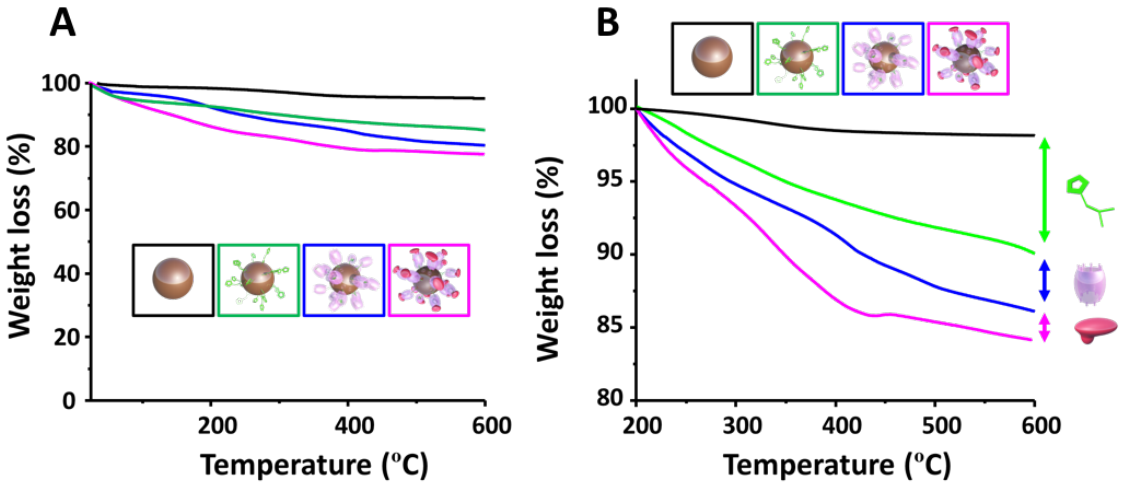

Figure S7. A) TGA curves (30 ºC to 600 ºC) and B) normalized TGA curves (200 ºC to 600 ºC) corresponding to the removal of the organic layer from **NPs** (black), **Z-NPs** (green), **CZ-NPs** (blue), and **DCZ-NPs** (pink).

TGA percentages were used to estimate the number of Zol, CB[7] and Dox per **NP**.

The number of nanoparticle in the sample was deduced using this formula:

$$N_{nano} = \frac{n_{NPs} \times M_{NPs}}{\rho \times \frac{4}{3} \times \pi \times R^3}$$

(*) Where R is 5 nm, the average **NP** radius obtained from TEM analysis, ρ is **NP** density, M_{NPs} is molar mass of Fe_2O_3, and n_{NPs} is the number of moles of **NPs** deduced from TGA.[1]

	Weight loss (%)	Mass in 1 g (g)	n in 1 g (mol)	Number of entities in 1 g
NPs	90.5	0.9	$N_{Fe}= 4.6\times10^{-3}$	$^{*}N_{nano}=2.4\times10^{17}$
Zol	9.5	0.09	3.5×10^{-4}	2.1×10^{20}

Table S1. TGA calculations for **Z-NPs**.

	Weight loss (%)	Mass in 1 g (g)	n in 1 g (mol)	Number of entities in 1 g
NPs	86.25	0.86	$N_{Fe}= 4.4\times10^{-3}$	$^{*}N_{nano}=2.4\times10^{17}$
Zol	9.05	0.09	3.3×10^{-4}	2.0×10^{20}
CB[7]	4.5	0.04	3.9×10^{-5}	2.3×10^{19}

Table S2. TGA calculations for **CZ-NPs**.

	Weight loss (%)	Mass in 1 g (g)	n in 1 g (mol)	Number of entities in 1 g
NPs	84.5	0.84	$N_{Fe}= 4.3\times10^{-3}$	$^{*}N_{nano}=2.3\times10^{17}$

Zol	8.87	0.09	3.2×10^{-4}	1.9×10^{20}
CB[7]	4.40	0.04	3.8×10^{-5}	2.3×10^{19}
Dox	1.75	0.01	3.1×10^{-5}	1.9×10^{19}

Table S3. TGA calculations for **DCZ-NPs**.

	Zol	**CB[7]**	**Dox**
Z-NPs	866	-	-
CZ-NPs	865	103	-
DCZ-NPs	866	106	83

Table S4. Number of molecules per **Z-NP**, **CZ-NP**, and **DCZ-NP**.

1.5. Control Experiments

1.5.1. - Determination of the average number of Zol molecules per nanoparticle using ^{31}P NMR spectroscopy

The average number of Zol molecules adsorbed per **Z-NP**, **CZ-NP**, and **DCZ-NP** was deduced using ^{31}P NMR spectroscopy.[1-3] Firstly, solutions having different but known concentrations of free Zol were prepared. Each of these was measured by ^{31}P NMR (80.9 MHz) along with an internal standard consisting of a capillary tube filled with 0.1 M NaH_2PO_4 in D_2O. The ^{31}P NMR signal intensity due to Zol was then plotted against Zol

concentration and used as a calibration curve (Figure S8). In order to determine the number of Zol molecules per nanoparticle, **Z-NPs**, **CZ-NPs**, and **DCZ-NPs** were decomposed in acidic medium (nitric acid 65%). The ferrous ions were removed by addition of sodium hydroxide NaOH (10^{-1} mol.L^{-1}) in order to prevent the iron from shifting the ^{31}P NMR signal of Zol. Sample supernatant was analyzed by ^{31}P NMR. The number of Zol molecules per **Z-NP**, **CZ-NP**, and **DCZ-NP** was obtained by dividing the number of Zol deduced by the corresponding number of nanoparticles in the solution analyzed. The number of nanoparticles in each sample was deduced from the iron concentration (ϵ_{480} = 420 L.mol^{-1}.cm^{-1}) of the sample using the following formula:

$$N_{nano} = \frac{n_{NPs} \times M_{NPs}}{\rho \times \frac{4}{3} \times \pi \times R^3}$$

(*) Where *R* is 5 nm, the average NP radius obtained from TEM analysis, ρ is NP density, M_{NPs} is the molar mass of Fe_2O_3, and n_{NPs} is the number of moles of NPs as deduced from TGA.[4]

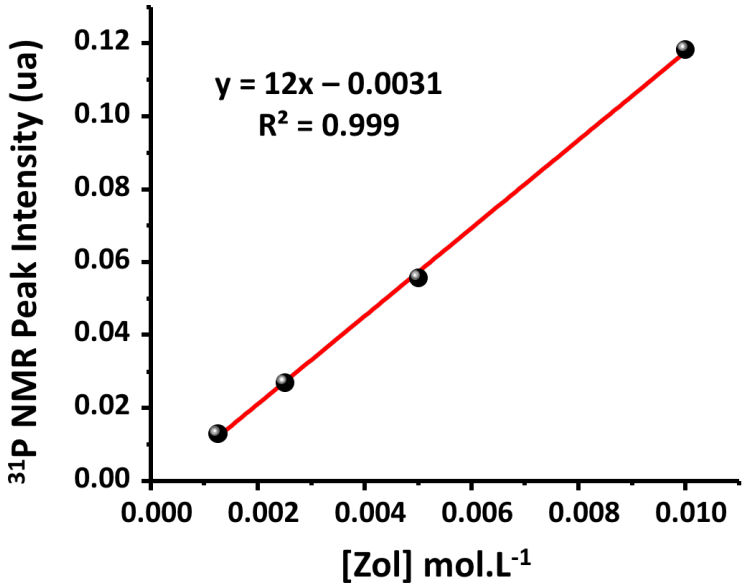

Figure S8. Calibration curve obtained by measuring the ^{31}P NMR signal intensity of Zol at different Zol concentrations. (80.9 MHz ^{31}P NMR, D_20, 298 K).

	Zol per NP (^{31}P NMR)	**Zol per NP (TGA)**
Z-NPs	981	866
CZ-NPs	909	865
DCZ-NPs	877	866

Table S5. Number of Zol molecules per **Z-NP** ([Fe] = 0.11 M), **CZ-NP** ([Fe] = 0.12 M), and **DCZ-NP** ([Fe] = 0.12 M) obtained by ^{31}P NMR and TGA analyses.

1.5.2. - Determination of the average number of Dox per DCZ-NP by fluorescence spectroscopy

Unloaded **CZ-NPs** are not intrinsically fluorescent at the Dox-specific excitation wavelength of λ_{ex} = 488 nm. At pH 7.4 and at λ_{ex} = 488 nm, **DCZ-NPs** fluoresce less than an aqueous sample of free Dox at the same drug concentration (quenching factor *Qf* = 3). This indicates that fluorescence quenching occurs within the **DCZ-NP** construct. Such quenching can be attributed to electronic interactions between the excited dye molecules and the **NPs**, or to self-quenching of the dye on the surface of the particles where the effective concentration of the dye is relatively high.

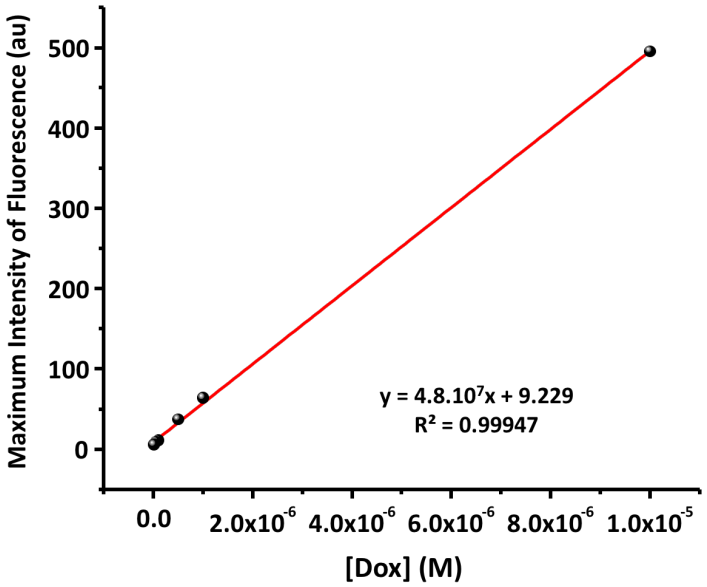

Figure S9. Calibration curve obtained by measuring the maximum fluorescence signal at different Dox concentrations (λ_{max} = 560 nm, H_20, 298 K).

The molar amount of Dox in **DCZ-NPs** was determined as follows. Dox was released from the particles by suspending them in an alkaline medium for 24 h. The particles were separated from the fluorescent supernatant by magnetic decantation. After dilution in water (dilution factor d = 300), Dox concentration was deduced at pH 7 by measuring Dox fluorescence and referring to a calibration curve (Figure S9).

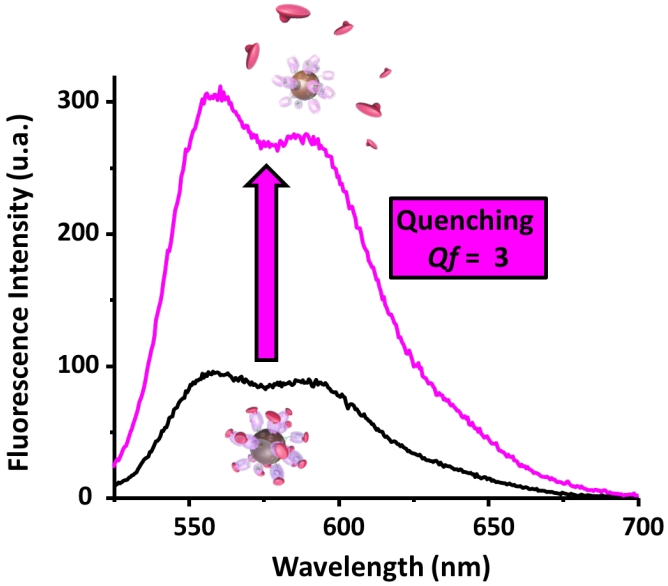

Figure S10. Fluorescence emission spectra of **DCZ-NPs** (black curve) and free Dox desorbed from **DCZ-NPs** (pink curve) in H_2O at pH 7.4 and 298 K and with λ_{ex} = 488 nm. The lower intensity of the fluorescence signal of **DCZ-NPs** (as compared to the signal from uncomplexed Dox) indicates fluorescence quenching.

	Dox per NP (fluorescence)	**Dox per NP (TGA)**
DCZ-NPs	98	83

Table S6. Number of Dox molecules per **DCZ-NP** ([Fe] = 0.2 M) obtained by fluorescence and TGA analyses.

1.6. Dynamic light scattering (DLS) characterization

DLS measurements were carried out on a Zetasizer Nano-ZS (Malvern Instruments) to determine the Zeta(ζ)-potential of the particles. All samples were analyzed at room temperature in water with diluted ferrofluid ([Fe] = 1×10^{-3} M).

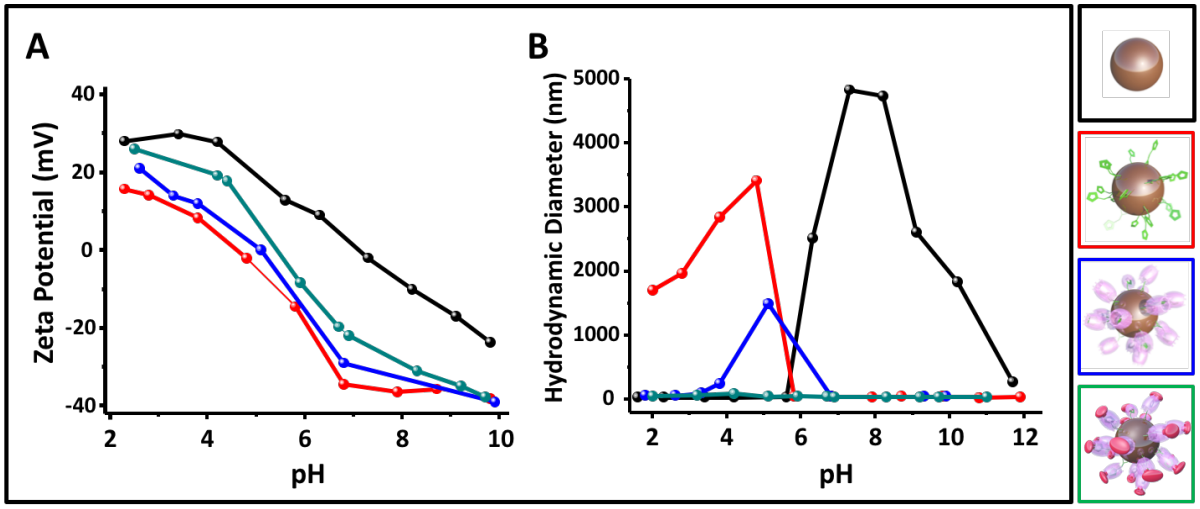

Figure S11. A) Zeta potential and B) hydrodynamic diameter of **NPs** (black), **Z-NPs** (red), **CZ-NPs** (blue), and **DCZ-NPs** (green) as a function of pH.

1.7. Control experiment

Z-NPs ([Fe] = 0.1 M, V= 5 mL) were mixed with Dox (m_{Dox} = 9.1 mg, n_{Dox} = $1.6.10^{-5}$ mol) in water at pH 7 and room temperature for 24 hours. The resulting brown **NP** precipitate was dialyzed for one day to remove uncomplexed Dox and was resuspended in water at pH 7.

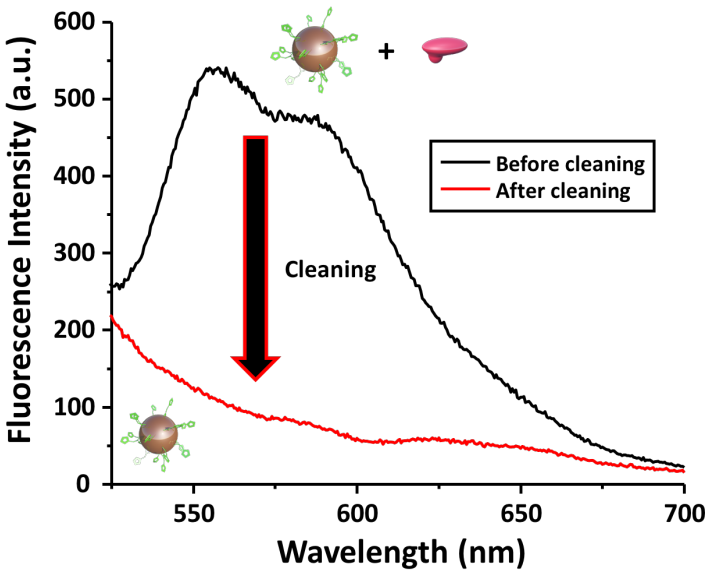

Figure S12. Fluorescence emission spectra of **Z-NPs** before and after the removal of free Dox using H_2O at pH 7.4 and 298 K and with λ_{ex} = 488 nm. The lack of fluorescence of the **NPs** after cleaning confirms the absence of uncomplexed Dox.

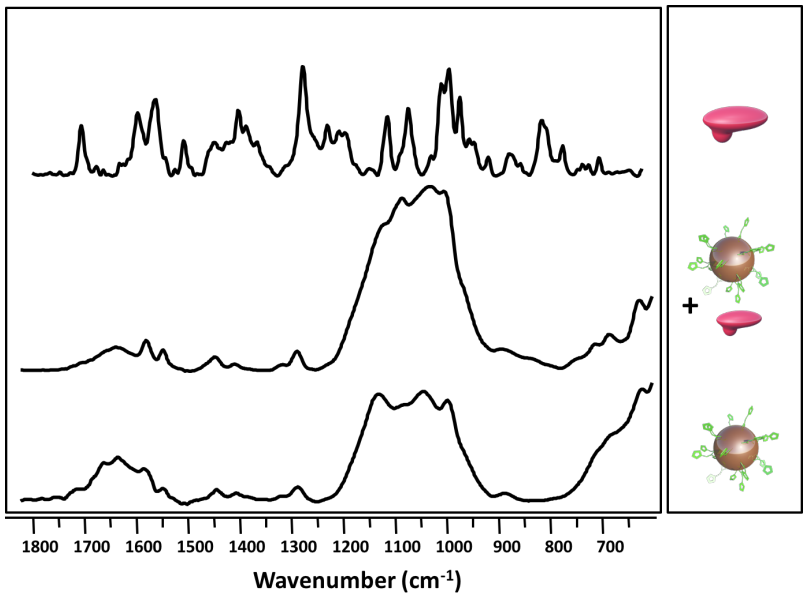

Figure S13. FTIR spectra of Dox (top), **Z-NPs** + free Dox (middle), and **Z-NPs** after the removal of free Dox by dialysis (bottom).

2. Release studies of Zol by ESI mass spectrometry

Solutions having a range of concentrations of free Zol were prepared to generate a calibration curve (Figure S14). The intensity of the *m/z* signal of the Zol molecular ion ($C_5H_9N_2O_7P^{2-}$ *m/z* calc = 270.98905, found = 270.99517) was plotted against the concentration of Zol .

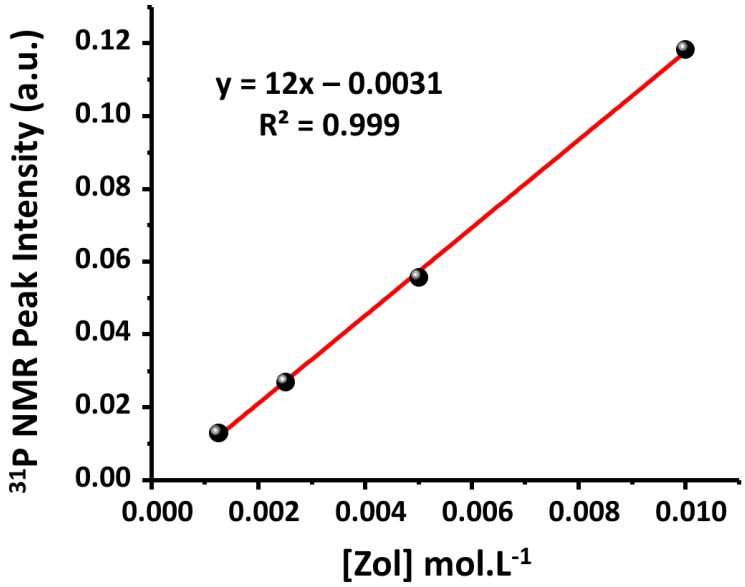

Figure S14. Calibration curve obtained by measuring the intensity of the *m/z* signal of the Zol molecular ion ($C_5H_9N_2O_7P^{2-}$ *m/z* calc = 270.98905, found = 270.99517) versus Zol concentration. (H_20, 298 K)

The gradual release of Zol from **DCZ-NPs** ([Fe] = 0.001M) was monitored in water at pH 7.4 and pH 5.4 over time by ESI mass spectrometry in the negative detection mode. The pH of the solutions was adjusted using a 1 M $HCl_{(aq)}$ solution. At regular intervals, solutions were centrifuged, supernatants were collected, and the intensity of the *m/z* signal was measured with reference to the calibration curve.

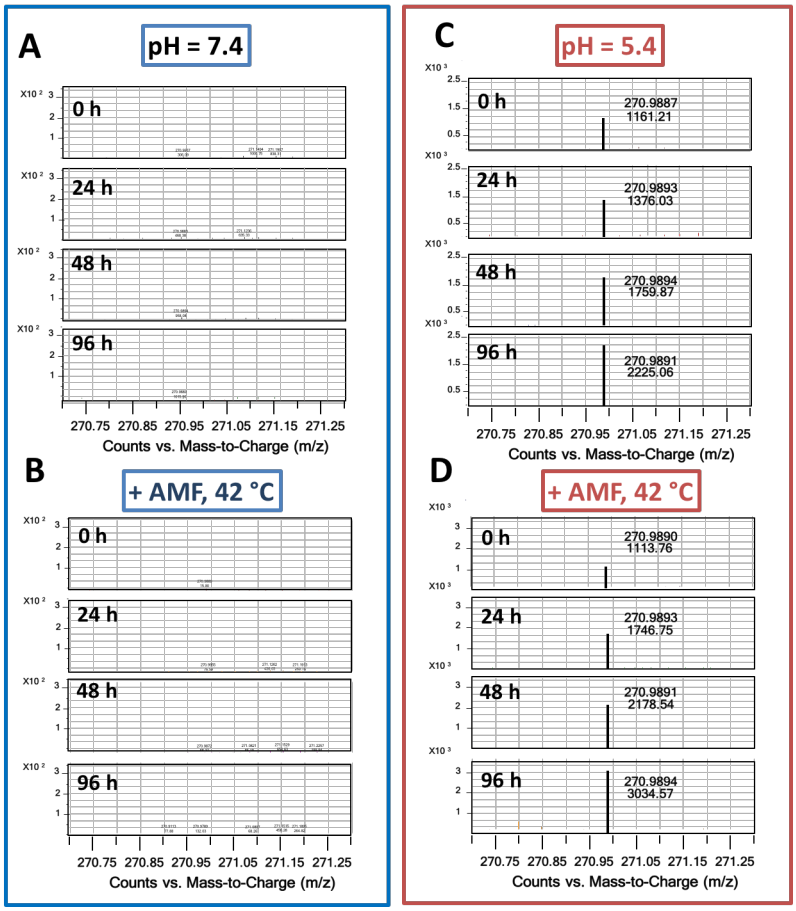

Figure S15. Zol release from **DCZ-NPs** monitored by ESI mass spectrometry in negative mode. Release is negligible at pH 7.4 and room temperature (A) as well as upon AMF-induced heating of the sample to 42 ºC (B). However, Zol release is gradual after adjustment of the pH to 5.4, either at room temperature (C) or when the sample is subjected to AMF-induced heating (464 kHz frequency, 26.8 kA m^{-1} amplitude) to 42 ºC (D).

3. Response of DCZ-NPs to heating induced by an alternating magnetic field (AMF) in solution

The effect of an AMF on the temperatures of solutions of **Z-NPs**, **CZ-NPs**, **DCZ-NPs** and uncoated **NPs** was investigated using a magneTherm system (NanoTherics). The device produces an alternating current (AC) magnetic field of frequency 464 kHz and a current of 26.8 kAm^{-1}. Samples of **NPs**, **Z-NPs**, **CZ-NPs** and **DCZ-NPs** ([Fe] = 0.08 M) were placed inside the magneTherm for two hours. The temperature of the samples was measured and recorded with respect to time using an external probe placed in the solutions.

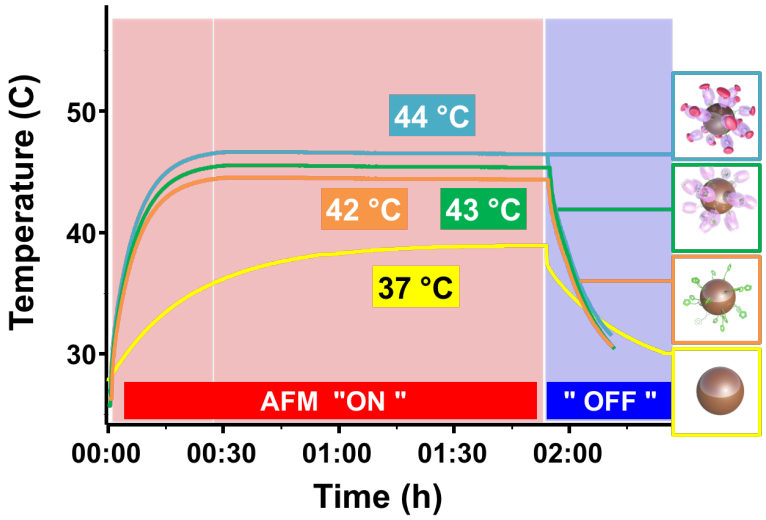

Figure S16. Temperature response curves for solutions (pH 7.4, [Fe] = 0.08 M) of bare **NPs** (yellow) **Z-NPs**, (orange) **CZ-NPs**, (green) **DCZ-NPs** (blue) in the presence and absence of AMF (464 kHz).

4. Biological studies

4.1. Cell culture

Breast cancer (MCF-7, ATCC No.HTB-22) and non-cancer (Human Embryonic Kidney 293, HEK; ATCC No. CRL-1573) cell lines were cultured in Dulbecco's Modified

Eagle's medium (DMEM), 10% fetal bovine serum (FBS), 1% penicillin/streptomycin and 20 mL L-glutamine at 5% CO_2 and 37 ºC.

4.2. Flow cytometry (FACS)

Cells were grown in petri dishes to a density of 100,000 cells/mL. They were incubated with no additives (control), with Dox alone ([Dox] = 0.2 μM) or with **DCZ-NPs** ([Zol] = 2 μM, [Dox] = 0.2 μM). One sample of **DCZ-NP**-treated cells was subjected to magnetically induced heating, and one was left unheated. Dox uptake was measured with a BD Accuri C6 flow cytometer.

4.3. Magnetic quantification of DCZ-NP uptake in MCF-7 cancer cells and HEK293 cells

The amount of **DCZ-NP** taken up by MCF-7 cancer cells and HEK293 cells was determined by measuring the nonlinear magnetization of the samples with a MIAtek reader.[5] In this assay, signal is proportional to the amount of magnetic particles present, and the reader can detect nanograms of particles. The mean number of **DCZ-NPs** per cell was obtained by dividing the total amount of iron measured with the reader by the number of cells. Biological samples exhibit only diamagnetism, a linear magnetic behavior that does not interfere with the measurement of nonlinear magnetization.

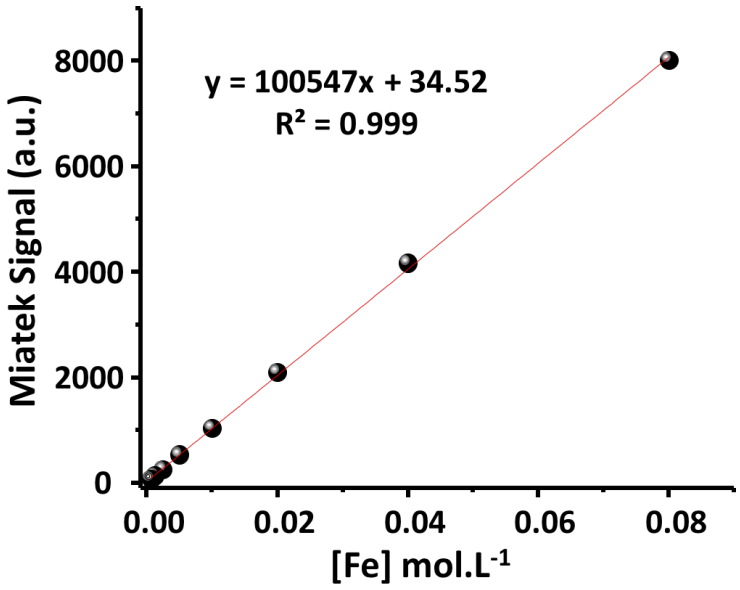

Figure S17. Calibration curve obtained by measuring the Miatek signal of **DCZ-NPs** at different iron concentrations.

4.4. *In vitro* cell viability assay

96-well plates were seeded with cells (~5,000 cells per well in 100 µL of DMEM) and incubated at 37 ºC for 24 hours. The medium was removed and replaced with fresh DMEM (control) or various concentrations of Dox, Zol, **Z-NPs**, **CZ-NPs**, or **DCZ-NPs** (up to 100 µM in Dox or Zol per sample) and incubated at 37 ºC for 48 hours. Thereafter, cells were washed with PBS and incubated with 20 µL of CellTiter-Blue® (CTB, Promega) reagent per well for six hours at 37 ºC. The fluorescence of the resofurin product ($\lambda_{ex/em}$ 560/620) was measured. Untreated wells were used as a control.

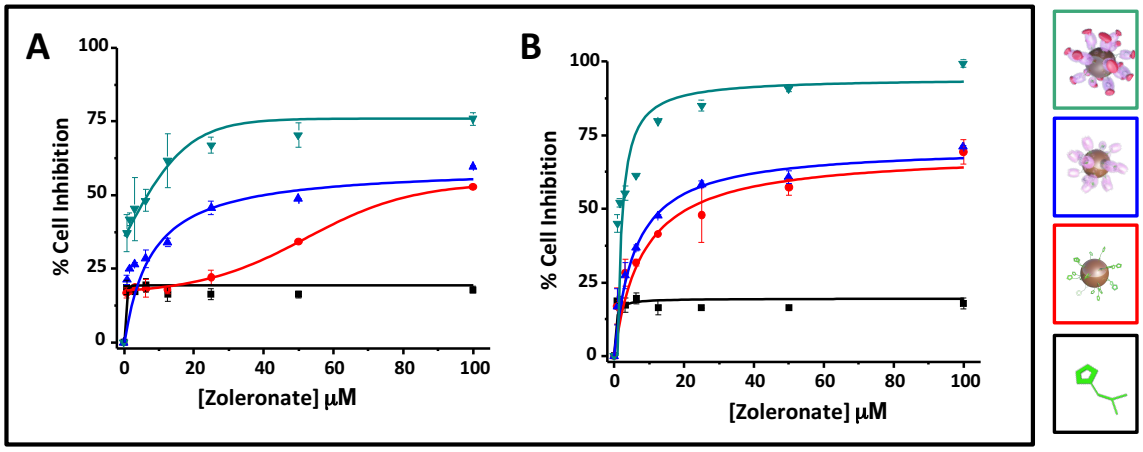

Figure S18. Inhibition of MCF-7 cells after 48 h incubation with Zol (black), **Z-NPs** (red), **CZ-NPs** (blue) and **DCZ-NPs** (green) in the absence (A) and presence (B) of a static magnetic field (neodyme magnet 0.2 T) up to [Zol] = 100 µM. Error bars represent standard deviations of triplicate measurements.

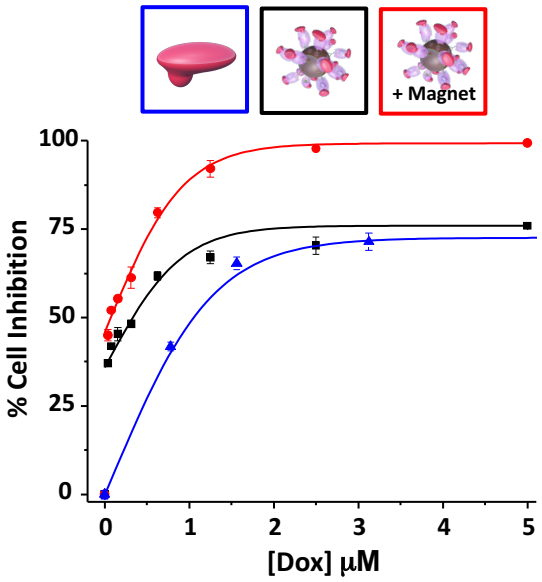

Figure S19. Inhibition of MCF-7 cells after 48 h incubation with Dox (blue), **DCZ-NPs** (black) or **DCZ-NPs** in the presence of a magnet (red). Error bars represent standard deviations of triplicate measurements.

4.5. Detection of apoptosis by dual Annexin V-FITC/PI staining.

MCF-7 cell apoptosis was studied using an Annexin V-fluorescein isothiocyanate (FITC) and propidium iodide (PI) apoptosis detection kit (BD Biosciences) and fluorescence activated cell sorting (FACS), according to the manufacturer's instruction. MCF-7 cells were seeded in 6-well plates in complete DMEM and incubated for 24 h before exposure to no additives (control), Zol, Dox, **Z-NPs**, **CZ-NPs** or **DCZ-NPs** for 24 h. The cells, including dead ones floating in the supernatant were then harvested and washed with PBS. The cells were then incubated in binding buffer with FITC (10 µl, 100 µg.ml^{-1}) for 60 min and binding buffer with PI (5 µl, 100 µg.ml^{-1}) for 5 min in the dark. Apoptotic cells were identified by flow cytometry. Each sample was assayed in duplicate, and the entire experiment was repeated three times.

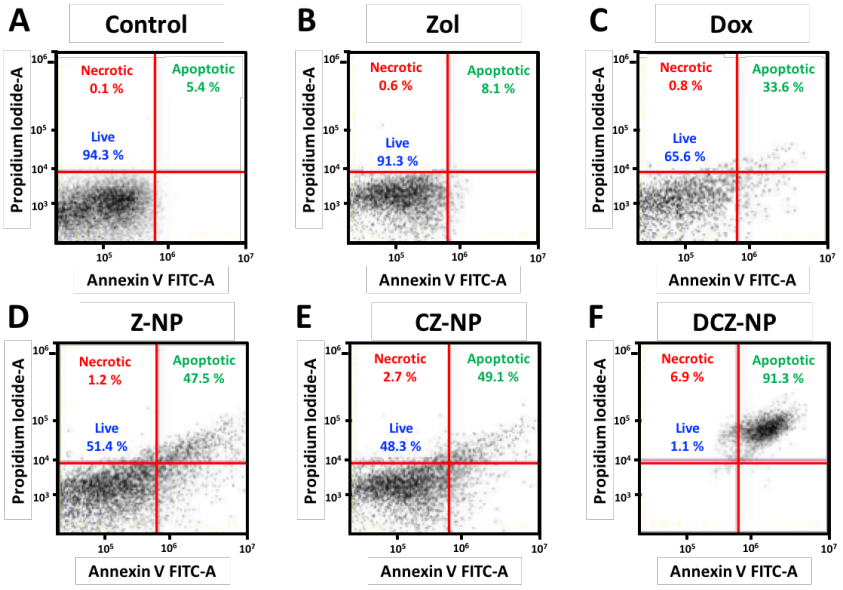

Figure S20. Flow cytometry measurements of MCF-7 cells treated with A) no additives (control), B) Zol ([Zol] = 5 µM), C) Dox ([Dox] = 0.5 µM), D) **Z-NPs** ([Zol] = 5 µM), E) **CZ-NPs** ([Zol] = 5 µM), and F) **DCZ-NPs** ([Zol] = 5 µM, [Dox] = 0.5 µM) for 24 hours

and stained with Annexin V-FITC and PI. Apoptotic cells include early apoptotic cells (Annexin V+/PI-) and late apoptotic cells (Annexin V+/PI+).

4.6. *In vitro* response of DCZ-NPs to AMF

The *in vitro* response of **DCZ-NPs** to AMF (frequency = 464 kHz, current = 26.8 kAm^{-1}) was measured. MCF-7 cells were seeded in two Petri-dishes (~50,000 cell/mL) and incubated for 24 hours. After 24 hours, the medium was replaced with fresh DMEM (control), or **DCZ-NPs** ([Zol] = 2 μM, [Dox] = 0.2 μM in DMEM) and incubated for two hours. Cells were washed three times with PBS, and fresh DMEM was added to the petri-dish. Cells were subjected to AMF for 30 minutes. An external probe placed in the medium recorded the temperature increase inside the petri dish that contained the cells.

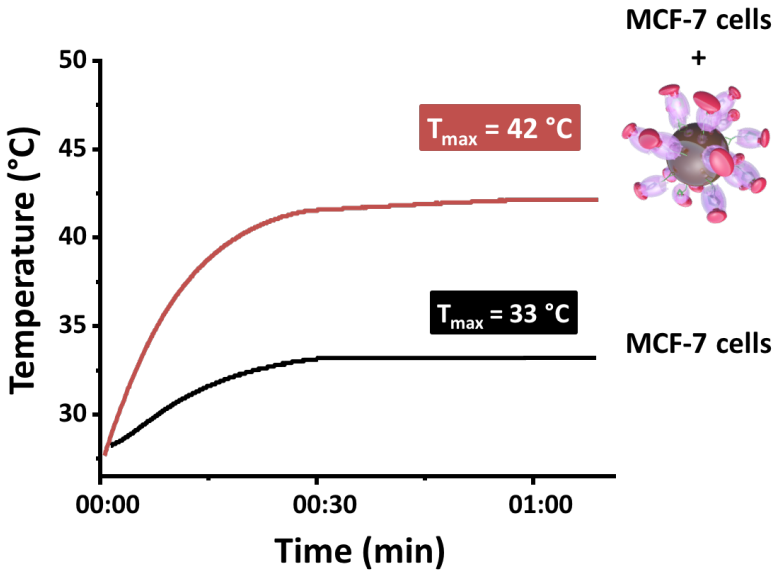

Figure S21. Variation of the temperature of the cell medium during 30 minutes of AMF application (frequency = 464 kHz, current = 26.8 kAm^{-1}, [Dox] = 0.2 μM) to MCF-7 cells (black curve) and MCF-7 cells incubated for two hours with **DCZ-NPs** (red curve).

4.7. *In vitro* hyperthermia treatment

Cell viability assays were performed to investigate the combined effect of both hyperthermia and chemotherapy treatments on MCF-7 cells. Petri-dishes were seeded with MCF-7 cells (~50,000 cells/mL) and incubated at 37 ºC for 24 hours. Cells were separated into two groups and incubated for two hours with cell-medium alone (control), or **DCZ-NPs** ([Zol] = 2 μM, [Dox] = 0.2 μM in DMEM). A sample from each treatment group was then subjected to an AMF (frequency = 464 kHz, current = 26.8 kAm^{-1}) for one hour to induce hyperthermia. The viability of unheated samples was measured immediately after incubation and 24 and 48 hours after incubation. The viability of heated samples was measured immediately after AMF removal and 24 and 48 hours after AMF removal. For cell viability studies, 200 μL CTB reagent per 1 mL of DMEM was added to each petri-dish. Cells were then incubated for six hours prior to fluorescence measurement.

5. Analysis of synergism

Therapies based on synergistic agents allow for reduced drug dosing and toxicity. Two agents act synergistically when their combined effect is greater than the sum of their individual effects. Chou and Talalay derived the combination index (CI) and median effect equation (MEE) in 1984 and have since established precedents for analyzing synergism.[6,7] The CI is the natural law–based general expression of pharmacologic drug interactions. It is shown to be the simplest possible way for quantifying synergism or antagonism.

The resulting combination index (CI) theorem of Chou-Talalay offers a quantitative definition for additive effect (CI = 1), synergism (CI < 1), and antagonism (CI > 1) in drug combinations.

The prerequisite is the dose-effect curves for each drug alone. Each drug not only has a different potency (the Dm value) but also a different shape of the dose-effect curve (the m value). For any determination of synergy, one needs to know both the potency and the shape of the dose-effect curve of each drug.

$$\mathrm{CI} = \frac{D_{\mathrm{comb},1}}{D_{\mathrm{alone},1}} + \frac{D_{\mathrm{comb},2}}{D_{\mathrm{alone},2}} + \propto \frac{D_{\mathrm{comb},1} D_{\mathrm{comb},2}}{D_{\mathrm{alone},1} D_{\mathrm{alone},2}}$$

Here, CI is the combination index; $D_{alone,1}$ is the dose of drug 1; $D_{alone,2}$ is the dose of drug 2; $D_{comb,1}$ is the combination dose of drug 1; and $D_{comb,2}$ is the combination dose of drug 2. For mutually nonexclusive drugs, $\propto = 1$, which corresponds to the case where the drugs have independent modes of action.

The determination of synergy *in vitro* and in animals follow the same principle and is why we used the values of IC_{50} measured previously to determine CI.

References

(1) Benyettou, F.; Lalatonne, Y.; Sainte-Catherine, O.; Monteil, M.; Motte, L. Superparamagnetic Nanovector with Anti-Cancer Properties: Γfe2o3@Zoledronate. *Int. J. Pharm.* **2009**, *379*, 324-327.

(2) Benyettou, F.; Lalatonne, Y.; Chebbi, I.; Benedetto, M. D.; Serfaty, J.-M.; Lecouvey, M.; Motte, L. A Multimodal Magnetic Resonance Imaging Nanoplatform for Cancer Theranostics. *Physical Chemistry Chemical Physics* **2011**, *13*, 10020-10027.

(3) Motte, L.; Benyettou, F.; de Beaucorps, C.; Lecouvey, M.; Milesovic, I.; Lalatonne, Y. Multimodal Superparamagnetic Nanoplatform for Clinical Applications: Immunoassays, Imaging & Therapy. *Faraday Discuss.* **2011**, *149*, 211-225.

(4) Verma, S.; Pravarthana, D. One-Pot Synthesis of Highly Monodispersed Ferrite Nanocrystals: Surface Characterization and Magnetic Properties. *Langmuir* **2011**, *27*, 13189-13197.

(5) Geinguenaud, F.; Souissi, I.; Fagard, R.; Motte, L.; Lalatonne, Y. Electrostatic Assembly of a DNA Superparamagnetic Nano-Tool for Simultaneous Intracellular Delivery and in Situ Monitoring. *Nanomedicine* **2012**, *8*, 1106-1115.

(6) Chou, T. C. Drug Combination Studies and Their Synergy Quantification Using the Chou-Talalay Method. *Cancer Res.* **2010**, *70*, 440-446.

(7) Chou, T. C.; Talalay, P. Quantitative Analysis of Dose-Effect Relationships: The Combined Effects of Multiple Drugs or Enzyme Inhibitors. *Adv. Enzyme Regul.* **1984**, *22*, 27-55.